INTERNATIONAL JOURNAL FOR NUMERICAL METHODS IN FLUIDS, VOL. 18, 647–668 (1994)

IMPLICIT SCHEMES FOR UNSTEADY EULER EQUATIONS ON TRIANGULAR MESHES

A. S. SENS AND G. D. MORTCHELEWICZ

Office National d'Etudes et de Recherches Aérospatiales, 29 Avenue de la Division Leclerc, F-92322 Chatillon, France

SUMMARY

An implicit finite element method is presented for the solution of steady and unsteady inviscid compressible flows on triangular meshes under transonic conditions. The method involves a first-order time-stepping scheme with a finite element discretization that reduces to central differencing on a rectangular mesh. On a solid wall the slip condition is prescribed and the pressure is obtained from an approximation of the normal momentum equation. With this solver no artificial viscosity is added to ensure the success of the calculation. Numerical examples are given for steady and unsteady cases.

KEY WORDS Euler equations Finite element method Implicit scheme Unsteady flow Transonic flow

1. INTRODUCTION

The problem of unsteady transonic flow is of great interest to aeroelasticians who have to determine unsteady aerodynamic loads on aerofoils over a wide range of Mach number and reduced frequency. A large number of calculation methods are based on the solution of transonic small-disturbance and full potential equations.[1–3]

Considerable progress has been made over the past decade in developing algorithms for the solution of the Euler and Navier–Stokes equations using unstructured meshes.[4–15] Many of the methods that are currently being developed are based on extensions of finite difference schemes constructed from Taylor expansions to unstructured meshes. The finite element method is then used to construct the space of approximation. The resultant unstructured grid flow solvers differ in terms of the time-dependent discretization, the integration rules, the boundary conditions or the artificial viscosity term used. Following this approach, we are interested in the family of centred implicit schemes of second order devised originally by Lerat[16–17] and Lerat *et al.*[18] and more recently by Lerat and Sidès.[19] With their last implicit centred scheme, Lerat and Sidès are able to calculate steady transonic flows with shock waves on structured grids without artificial viscosity. Our work consists of developing an implicit scheme for unstructured meshes which has the same property.

An algorithm for the solution of the time-dependent Euler equations is presented for unsteady aerodynamic analysis of oscillating aerofoils. This algorithm is developed for use on an unstructured mesh made up of triangles. This scheme can be implemented in two phases, one explicit and one implicit, which arise at each time step. The explicit stage is a two-step, second-order-accurate one and the implicit stage is based on the spectral radius method of Lerat *et al.*[18]

A finite element discretization is then applied to the time-dependent scheme, with specific integration rules to compute non-linear terms. The linear system which results from the

CCC 0271–2091/94/070647–22

Received July 1992
Revised November 1993

implicit stage is resolved component by component using a preconditioned conjugate gradient method.

The numerical method is slightly modified for unsteady applications following the approach developed by Sens[20] on structured grids. Finally, some theoretical results are given in the 1D case for both steady and unsteady methods.

Another aspect of the work concerns wall boundary conditions, which are treated here in a strong way. First we consider the special case of a solid fixed wall on which the slip condition is prescribed; we indicate the procedure used to calculate the pressure. To treat aeroelastic problems on a fixed mesh, we modify the solid wall boundary conditions in order to introduce a small displacement or deformation hypothesis. We present the approach used to calculate the pressure in full detail. In both steady and unsteady cases the complete boundary field is determined by extrapolation.

In order to assess the Euler solver and the wall boundary conditions, calculations were performed for two AGARD aerofoils in the frequently critical transonic speed regime. With this solver no artificial viscosity is added to ensure the success of the calculation.

2. GOVERNING EQUATIONS

The equations under consideration are the compressible Euler equations, which can be written for a two-dimensional flow with respect to a Cartesian co-ordinate system (x, y) as

$$w_t + f(w)_x + g(w)_y = 0, \tag{1}$$

where

$$w = \begin{pmatrix} \rho \\ \rho u \\ \rho v \\ E \end{pmatrix}, \qquad f(w) = \begin{pmatrix} \rho u \\ \rho u^2 + P \\ \rho uv \\ (E + P)u \end{pmatrix}, \qquad g(w) = \begin{pmatrix} \rho v \\ \rho uv \\ \rho v^2 + P \\ (E + P)v \end{pmatrix}.$$

The subscripts t, x and y in equation (1) denote the time and space partial derivatives, with $(x, y) \in \Omega \subset \mathbb{R}^2$, Ω being a bounded fixed open set delimited by Γ, the connection of boundaries which are supposed to be of class C^0 and C^1 by parts.

Here u and v denote the velocity components with respect to the Cartesian co-ordinate system, ρ is the density, P is the pressure and $E = \rho e$, e being the total energy. The equation set is completed by the addition of an equation of state; assuming the fluid to be an ideal gas, this takes the form

$$P = (\gamma - 1)[E - \tfrac{1}{2}\rho(u^2 + v^2)],$$

where γ is the ratio of the specific heats. The problem to be solved is then defined by the specification of appropriate boundary conditions.

We denote $A(w)$ and $B(w)$ the Jacobian matrices of the flux functions, i.e.

$$A(w) = \frac{\mathrm{d}f}{\mathrm{d}w}(w), \qquad B(w) = \frac{\mathrm{d}g}{\mathrm{d}w}(w).$$

We denote $U \cdot V$ the Euclidean scalar product of U and V in $\mathbb{R}^2$ and $\| U \|$ the associated norm.

3. IMPLICIT SOLUTION ALGORITHM

The time-stepping scheme adopted here derives from the family of centred implicit schemes of second order devised originally by Lerat and co-workers.[16–19]

This scheme can be implemented in two phases which arise at each time step. In Δ-form one gets

(i) *explicit stage*

$$\Delta\tilde{w} = -\Delta t(f_x^n + g_y^n) + \frac{\Delta t^2}{2}\{[A^n(f_x^n + g_y^n)]_x + [B^n(f_x^n + g_y^n)]_y\}, \tag{2}$$

(ii) *implicit stage*

$$\Delta w + \beta\frac{\Delta t^2}{2}[(A^n)^2(\Delta w)_x + A^nB^n(\Delta w)_y]_x + \beta\frac{\Delta t^2}{2}[B^nA^n(\Delta w)_x + (B^n)^2(\Delta w)_y]_y = \Delta\tilde{w}, \tag{3}$$

(iii) *updating*

$$w^{n+1} = w^n + \Delta w,$$

where, $A^n = A(w^n)$, $B^n = B(w^n)$, $f^n = f(w^n)$, $g^n = g(w^n)$, $\Delta w = w^{n+1} - w^n$, w^n is the numerical solution at time level $t = n\Delta t$ and β is a real parameter.

The algorithm described above possesses excellent accuracy characteristics with appropriate space approximation.[19] However, when it is applied to systems of equations, it has the disadvantage of requiring the evaluation and subsequent multiplication of the matrices A and B, especially in its implicit stage. These operations are very time-consuming.

In order to avoid this, the computation of the explicit stage (2) is organized in a two-step fashion which can be shown to have the same order of accuracy.[21] The implicit stage (3) is then simplified. The crossed derivatives are suppressed and the spectral radii ρ_A and ρ_B are substituted for the matrices A and B. These simplifications do not alter the formal order of accuracy, since the implicit term is of the order of Δt^3.

Clearly we obtain

(i) *explicit stage*

(a) predictor

$$w^{n+\alpha} = w^n - \alpha\Delta t(f_x^n + g_y^n), \tag{4}$$

(b) corrector

$$\Delta\tilde{w} = -\Delta t(f_x^n + g_y^n) - \frac{\Delta t}{2\alpha}[(\tilde{f}^{n+\alpha} - f^n)_x + (\tilde{g}^{n+\alpha} - g^n)_y], \tag{5}$$

(ii) *implicit stage*

$$\Delta w + \beta\frac{\Delta t^2}{2}[(\rho_A^2\Delta w_x)_x + (\rho_B^2\Delta w_y)_y] = \Delta\tilde{w}, \tag{6}$$

where $\tilde{f}^{n+\alpha} = f(w^{n+\alpha})$ and α is a real parameter.

We can note that the term $\Delta\tilde{w}$ as defined in equations (4) and (5) is just the increment which results from applying the explicit Runge–Kutta scheme of second order to equation (1). The two-steps form (4), (5) is commonly used with the choice of 0·5 as the value for α[4,5,7,12].

4. FINITE ELEMENT DISCRETIZATION

The spatial solution domain Ω is a bounded polygonal domain whose boundary is denoted by Γ. A triangulation $\mathscr{T}_h$ with characteristic mesh spacing h is introduced on Ω. The vertices of the triangles define a set of computation nodes, S, where the numerical solution of (1) is to be computed. From $\mathscr{T}_h$, we derive a space $\mathscr{C}$ of functions which are piecewise linear on each triangle T of $\mathscr{T}_h$ and continuous on Ω. The set $(N_i)_i$ is a basis of $\mathscr{C}$ defined to be such that

$$N_i = \begin{cases} 1 & \text{at node } S_i, \\ 0 & \text{at all other nodes.} \end{cases}$$

A space $\mathscr{M}$ of functions which are piecewise constant on each element T of $\mathscr{T}_h$ is also introduced. The set $(\Pi_T)_{T \in \mathscr{T}_h}$ is a basis of $\mathscr{M}$:

$$\Pi_T(x, y) = \begin{cases} 1 & \text{if } (x, y) \in T, \\ 0 & \text{elsewhere.} \end{cases}$$

Multiplying (4) by Π_T and integrating by parts, we get for each triangle T

$$\int_T w^{n+\alpha} \, dx \, dy = \int_T w^n \, dx \, dy - \alpha \Delta t \int_{\partial T}^{*} (f^n n^x + g^n n^y) \, d\sigma, \tag{7}$$

where ∂T and $n = (n^x, n^y)$ denote respectively the boundary of element T and the outward vector normal to ∂T.

Multiplying (5) and (6) by N_i and integrating over Ω, one gets for each node S_i of $\mathscr{T}_h$

$$\int_\Omega \Delta \tilde{w} N_i \, dx \, dy = \Delta t \int_\Omega^{*} \left(f^n \frac{\partial N_i}{\partial x} + g^n \frac{\partial N_i}{\partial y} \right) dx \, dy + \frac{\Delta t}{2\alpha} \int_\Omega^{**} \left((\tilde{f}^{n+\alpha} - f^n) \frac{\partial N_i}{\partial x} + (\tilde{g}^{n+\alpha} - g^n) \frac{\partial N_i}{\partial y} \right) dx \, dy, \tag{8}$$

$$\int_\Omega \left[\Delta w N_i - \beta \frac{\Delta t^2}{2} \left(\rho_A^2 \Delta w_x \frac{\partial N_i}{\partial x} + \rho_B^2 \Delta w_y \frac{\partial N_i}{\partial y} \right) \right] dx \, dy = \int_\Omega \Delta \tilde{w} N_i \, dx \, dy, \tag{9}$$

where the upper indices $_*$ and $_{**}$ correspond to numerical integrations which are given further on.

Here Dirichlet conditions have been imposed on the boundary Γ. The integral over the surface Γ of the domain Ω then vanishes when the divergence theorem is applied to equations (8) and (9).

In the explicit stage (7), (8) the quadrature formulations used to compute non-linear terms are

$$\int_T^{*} F \, dx \, dy = \left(\sum_{i=1}^{3} \tfrac{1}{3} F_i \right) \text{meas}(T), \tag{10}$$

$$\int_T^{**} F \, dx \, dy = F(S_G) \, \text{meas}(T), \tag{11}$$

where F_i is the S_i-nodal value of F on element T and S_G is the element centre of gravity.

Remarks

With these choices for the numerical integration we obtain the same formulation for the predictor (7) as Zienkiewicz *et al.*[5] or Koschel *et al.*[7]

In the weak formulation Dirichlet conditions have been imposed. The procedure used to determine the unknowns on a wall is presented further on.

The explicit formulation (7), (8) with the choice (10), (11) comes from results established by Lerat[22] in the 1D case on explicit schemes. It differs from the formulation previously described in Reference 12. These two formulations will be compared further in the 1D case.

The linear system which results from (9) is resolved component by component using a preconditioned conjugate gradient method. Since the implicit matrix of (9) is a symmetric positive definite matrix, we compute only a local upper triangular matrix on each element. In order to preserve a reasonable size memory, the matrix is not assembled. As preconditioner matrix we use the diagonal matrix of (9). The algorithm is initialized from the explicit lumped mass matrix.[23] Desirable vectorization properties can be exploited if volume elements are arranged in coloured groups defined such that two elements of the same group have no common nodes.

5. UNSTEADY CASE

The implicit method (7)–(9) must be modified for unsteady applications. The procedure used follows the approach developed by Sens[20] on structured grids.

The implicit method of second-order accuracy proposed here has a time step that is not limited by the Courant–Friedrich–Levy (CFL) condition. In order to accelerate the convergence to the steady state, local time stepping is used. The method then has an internal dissipation which is sufficient to ensure the success of the calculation without any artificial viscosity.

For unsteady applications a global time step must be used because of the time accuracy requirement. For solutions with large gradients concentrated in narrow regions, meshes with a large variation in element size must be constructed. The global time step will be governed by the portions of the mesh that have the smallest spacing. As a consequence, a very small element Courant number is obtained for those portions of the mesh where the node spacing is large. The internal dissipation is no longer sufficient everywhere and some spurious oscillations can appear. To increase the internal dissipation in unsteady applications, we modify the time step Δt^2 connected with the second-order implicit term in (9) by

$$\Delta t^2 \rightarrow \tfrac{1}{2}(\Delta t + \Delta t_T)\Delta t$$

and the time step which arises in (7) by

$$\Delta t \rightarrow \tfrac{1}{2}(\Delta t + \Delta t_T),$$

where Δt_T is the local time step defined on T.

The method has formally first-order accuracy in time. However, it is possible to have locally second-order accuracy if we define

$$\Delta t = \min_T \Delta t_T.$$

6. 1D PROBLEMS

The domain Ω is divided into a set of non-overlapping subintervals with equal-length elements h. The scheme (7)–(9) leads to the following equations at node j of the mesh:

(i) *explicit stage*

$$w_{j+1/2}^{n+\alpha} = w_{j+1/2}^{n} - \alpha\sigma(f_{j+1}^{n} - f_{j}^{n}), \tag{12}$$

$$\Delta\tilde{w}_{Rj} = -\frac{\sigma}{2\alpha}\left[\tilde{f}_{j+1/2}^{n+\alpha} - \tilde{f}_{j-1/2}^{n+\alpha} + (2\alpha - 1)(f_{j+1/2}^{n} - f_{j-1/2}^{n})\right], \tag{13a}$$

$$\Delta\tilde{w}_{Sj} = -\frac{\sigma}{2\alpha}\left[\tilde{f}_{j+1/2}^{n+\alpha} - \tilde{f}_{j-1/2}^{n+\alpha} - f_{j+1/2}^{n} + f_{j-1/2}^{n} + \alpha(f_{j+1} - f_{j-1})\right], \tag{13b}$$

(ii) *implicit stage*

$$\Delta w_j + \tfrac{1}{6}(\Delta w_{j+1} - 2\Delta w_j + \Delta w_{j-1}) + \beta(\sigma^2/2) \left[(\rho_A^2)_{j+1/2}(\Delta w_{j+1} - \Delta w_j) - (\rho_A^2)_{j-1/2}(\Delta w_j - \Delta w_{j-1})\right] = \Delta\tilde{w}_j, \tag{14}$$

where $\tilde{f}_{j+1/2}^{n+\alpha} = f(w_{j+1/2}^{n+\alpha})$, $f_{j+1/2}^{n} = f(w_{j+1/2}^{n})$ and $\sigma = \Delta t/h$.

The subscripts R in equation (13a) and S in equation (13b) correspond to different discretizations of the non-linear terms in equation (9).

Several choices are possible for the discretization of the non-linear terms and lead to distinct approximations. In equation (13a) the numerical integration is performed using equation (11), while equations (10) and (11) are used to obtain formulation (13b). The scheme (12), (13b) is a variant of S_β^α schemes.

In the particular case described here we can note that[22]

the steady weak solutions of the exact system (1) *given by* $f(w) =$ *constant are solutions of the scheme* (12), (13*b*) *and conversely. This is not the case for the scheme* (12), (13*a*).

The second difference comes from integration rules used to calculate the flux f at the point $x = (j + \frac{1}{2})\delta x$. We denote trapezoidal and midpoint rules respectively by

$$\bar{f}(w) = \tfrac{1}{2}(f_j + f_{j+1}),$$

$$f(\bar{w}) = f\left(\frac{w_j + w_{j+1}}{2}\right).$$

Assuming that f and w can be written as Taylor expansions around the nearby origin (x_i, t_n), one gets the relation

$$\bar{f}(w) - f(\bar{w}) = \frac{\delta x^2}{8} f''(w)(w_x, w_x) + O(\delta x^3), \tag{15}$$

where $f''(w)$ is a bilinear application of R^m. A positive term occurs on the right-hand side of equation (15) which may be interpreted as a dissipative term.

In the linear case these schemes are identical and belong to the family of second-order implicit methods of Lerat[17,22] which have the following properties.

The implicit scheme (12)–(14) *is linearly stable, linearly dissipative (except at a point where A is singular) and linearly SDD (strictly diagonally dominant) without any conditions on the CFL number and if only if the parameter* β *is chosen as*

$$\beta \leqslant -\tfrac{1}{2}$$

For unsteady applications the implicit scheme can be written as

(i) *explicit stage*

$$w_{j+1/2}^{n+\alpha} = w_{j+1/2}^{n} - \alpha \frac{\sigma}{2}\left(\frac{\sigma'}{\sigma} + 1\right)(f_{j+1}^{n} - f_{j}^{n}),$$

$$\Delta\tilde{w}_{Sj} = -\frac{\sigma}{2\alpha}\left[\tilde{f}_{j+1/2}^{n+\alpha} - \tilde{f}_{j-1/2}^{n+\alpha} - f_{j+1/2}^{n} + f_{j-1/2}^{n} + \alpha(f_{j+1} - f_{j-1})\right],$$

(ii) *implicit stage*

$$\Delta w_j + \tfrac{1}{6}(\Delta w_{j+1} - 2\Delta w_j + \Delta w_{j-1}) + \beta\frac{\sigma^2}{4}\left(\frac{\sigma'}{\sigma} + 1\right)$$

$$[(\rho_A^2)_{j+1/2}(\Delta w_{j+1} - \Delta w_j) - (\rho_A^2)_{j-1/2}(\Delta w_j - \Delta w_{j-1})] = \Delta\tilde{w}_j,$$

where $\sigma' = \Delta t_T/h$.

Proposition

The unsteady implicit scheme is linearly stable, linearly dissipative (except at a point where A is singular) and linearly SDD (strictly diagonally dominant) without any condition on the CFL number if and only if the parameter β and the time step $\Delta t'$ are chosen as

$$\beta \leqslant -\tfrac{1}{2} \quad \text{and} \quad \Delta t' \geqslant \Delta t.$$

7. BOUNDARY CONDITIONS

Here we consider domains of computation related to external flows around bodies. The boundary Γ breaks down into a subsonic inflow or outflow boundary and a solid wall. In order to calculate the field w on each of these boundaries, we must consider the conditions to be prescribed and those to be calculated.

For the 2D Euler equations the set of these conditions must constitute a system of four linearly independent equations. We shall refer to this as a strong application of boundary conditions as opposed to a weak treatment.

The treatments used to calculate 'numerical' boundary conditions are e.g. extrapolation or the method of compatibility relations due to Viviand and Veuillot.[24]

In the case of a fluid boundary (inflow or outflow) the parameters are extrapolated according to the mesh lines.[12]The particular case of a solid wall is now discussed in the context of the steady flow around a fixed body and then in the case of the unsteady flow over a moving wall.

Let s_1, s_2 and s_3 be the local vertices of an element T which intersects Γ (see Figure 1), $\partial T = \partial T_{12} \cup (\partial T_{13} \cup \partial T_{23})$ be the boundary of T, $\bar{w} = (\bar{\rho}, \bar{A}, \bar{B}, \bar{E})$ be the field on ∂T_{12} with $\bar{A} = \bar{\rho}\bar{u}$ and $\bar{B} = \bar{\rho}\bar{v}$, $\bar{V} = (\bar{u}, \bar{v})$ be the fluid velocity and $w_i = (\rho_i, A_i, B_i, E_i)$ be the field at node S_i.

7.1. *Boundary condition: fixed wall*

On a rigid wall the slip condition is prescribed as

$$\bar{V}\cdot n = 0 \tag{16}$$

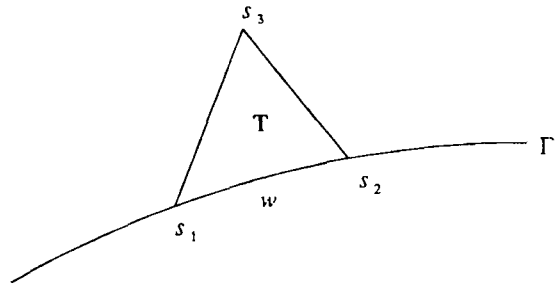

Figure 1. Computation of the slip condition

and the numerical flux depends only on the pressure, i.e.

$$\int_{\partial T_{12}} (fn^x + gn^y)\,\mathrm{d}\sigma = P\begin{pmatrix} 0 \\ n^x \\ n^y \\ 0 \end{pmatrix}, \tag{17}$$

where $n = (n^x, n^y)$ denotes the outward vector normal to ∂T_{12}.

The procedure adopted here to calculate the pressure follows an approach advocated by Lerat and Sidès[19,25] for their implicit scheme.

On each triangle T of Ω which intersects Γ we can write the contribution of the boundary integral which results at the steady state:

$$\int_{\partial T} (fn^x + gn^y)\,\mathrm{d}\sigma = 0$$

or

$$\bar{P}\begin{pmatrix} 0 \\ n^x \\ n^y \\ 0 \end{pmatrix} = -\int_{\partial T_{13} \cup \partial T_{23}} (f^n n^x + g^n n^y)\,\mathrm{d}\sigma. \tag{18}$$

The pressure is then obtained from a linear combination of the discrete form of the x- and y-momentum equations as

$$\bar{P}(n^x)^2 + \bar{P}(n^y)^2 = -(F_u^n n^x + F_v^n n^y), \tag{19}$$

where the fluxes F_u^n and F_v^n denote the second and third components of the right-hand side of equation (18) respectively.

One gets for the pressure

$$\bar{P} = \frac{-1}{(n^x)^2 + (n^y)^2}(F_u^n n^x + F_v^n n^y). \tag{20}$$

On a boundary element the field $\bar{w} = (\bar{\rho}, \bar{A}, \bar{B}, \bar{E})^{\mathrm{T}}$ is obtained by extrapolating quantities such as the entropy, enthalpy and fluid velocity direction. The field w_i at node S_i is then defined as the mean of $\bar{w}$ on the left and right sides of node S_i, weighted by non-uniform mesh spacings.

7.2. Boundary condition: moving wall

For a mobile solid wall boundary the slip condition must be written as

$$(\bar{V} - \bar{V}_p) \cdot n(t) = 0, \tag{21}$$

where $\bar{V}_p = \bar{V}_p(t)$ and $n(t)$ denote the velocity and the instantaneous normal of the aerofoil on the surface of the wall respectively.

An exact formulation can be used to compute the case of motion of a rigid body or a deformable body.[17] In the case of motion of a deformable body, however, a variable mesh must be used over time as was done in Reference 26. In the framework of aeroelastic applications it is legitimate to introduce a hypothesis of small displacement or deformation, which allows an invariable mesh to be used through time in all cases as was done in References 12 and 27. In this case the motion is then taken into account using a blowing condition on the wall.

The procedure used to calculate the pressure P on a fixed wall was extended to the unsteady case in Reference 20 for the problem of rigid body motion on structured grids. Here we propose to extend this algorithm to unstructured meshes.

On each triable T of Ω which intersects Γ we approximate the system of Euler equations in intetral form as

$$\text{meas}(T)\Delta\bar{w} = -\Delta t \int_{\partial T} F(\bar{w}, n)\, d\sigma, \tag{22}$$

where $F(\bar{w}, n)$ denotes the flux at time level $t = (n + 1)\Delta t$:

$$F(\bar{w}, n) = (\bar{V} \cdot n)\bar{w} + \bar{P} \begin{vmatrix} 0 \\ n^x \\ n^y \\ \bar{V} \cdot n \end{vmatrix} \tag{23}$$

As before, we split the right-hand side of (22) in such a way that the boundary flux on ∂T_{12} appears. The two scalar equations of interest correspond to momentum equations as in the case of a fixed wall. Using the result of (23), we thus have

$$(\bar{A} - \bar{A}^n)\,\text{meas}(T) = -\Delta t[F_u^n + \bar{A}(\bar{V} \cdot n) + \bar{P}n^x], \tag{24}$$

$$(\bar{B} - \bar{B}^n)\,\text{meas}(T) = -\Delta t[F_v^n + \bar{B}(\bar{V} \cdot n) + \bar{P}n^y], \tag{25}$$

where F_u^n and F_v^n are the second and third components of the numerical flux over $\partial T_{23} \cup \partial T_{13}$ respectively. In equations (24) and (25) the pressure $\bar{P}$, the normal n and the scalar $\bar{V} \cdot n$ are those defined on ∂T_{12}; they are taken into account at time level $t = (n + 1)\Delta t$ like the components $\bar{A}$ and $\bar{B}$ without the upper index.

Multiplying (24) by n^x and (25) by n^y and summing leads to the equation

$$\bar{P}[(n^x)^2 + (n^y)^2] = -\frac{\text{meas}(T)}{\Delta t}[(\bar{A} - \bar{A}^n)n^x + (\bar{B} - \bar{B}^n)n^y] - F_u^n n^x - F_v^n n^y - (\bar{V} \cdot n)(\bar{A}n^x + \bar{B}n^y). \tag{26}$$

To proceed further, we must approximate $\bar{V} \cdot n$ and the density $\bar{\rho}$.

Let n and τ be the fixed normal and tangent basis vectors respectively of the boundary ∂T_{12}, with $\|n\| = \|\tau\|$, and $n(t)$ and $\tau(t)$ be the instantaneous normal and tangent basis vectors respectively of ∂T_{12} at time level $t = (n + 1)\Delta t$, with $\|n(t)\| = \|\tau(t)\|$.

The fluid velocity $\bar{V}$ on the local basis n, τ can be written as

$$\bar{V}\|n\|^2 = (\bar{V}\cdot n)n + (\bar{V}\cdot \tau)\tau. \tag{27}$$

Multiplying (27) by $n(t)$ and using the slip condition (21) gives

$$[\bar{V}_p \cdot n(t)]\|n\|^2 = (\bar{V}\cdot n)n\cdot n(t) + (\bar{V}\cdot \tau)\tau \cdot n(t).$$

Thus we have

$$\bar{V}\cdot n = \frac{1}{n\cdot n(t)}\,[\|n\|^2 \bar{V}_p \cdot n(t) - (\bar{V}\cdot \tau)^n \tau \cdot n(t)], \tag{28}$$

where the tangent fluid velocity is now evaluated at time level $t = n\Delta t$.

The density $\bar{\rho}$ can be expressed by constructing an approximation of first order in time and using the equation of continuity. We thus have

$$(\bar{\rho} - \bar{\rho}^n)\ \mathrm{meas}(T) = -\Delta t[F_\rho^n + \bar{\rho}(\bar{V}\cdot n)]$$

or

$$\bar{\rho}[\mathrm{meas}(T) + \Delta t(\bar{V}\cdot n)] = \bar{\rho}^n\ \mathrm{meas}(T) - \Delta t F_\rho^n. \tag{29}$$

The results of equations (28) and (29) are introduced into equation (27) to give the pressure.

In order to determine the field $\bar{w}$ on the boundary, we extrapolate the entropy σ_3 and the enthalpy H_3 from internal node s_3. One gets

$$\bar{\rho} = \left(\frac{\bar{P}}{\sigma_3}\right)^{1/\gamma}, \qquad \bar{E} = \bar{\rho}\left(H_3 - \frac{\bar{P}}{\bar{\rho}}\right), \qquad \bar{V}^2 = 2\left(H_3 - \frac{\gamma}{\gamma - 1}\,\frac{\bar{P}}{\bar{\rho}}\right). \tag{30}$$

The fluid velocity $\bar{V}$ is now decomposed on the instantaneous basis $n(t)$, $\tau(t)$ and the slip condition (21) is used to give

$$\bar{V}\|n(t)\|^2 = (\bar{V}_p \cdot n(t))n(t) + (\bar{V}\cdot \tau(t))\tau(t). \tag{31}$$

From (30) and (31) we can express

$$\|\bar{V}\cdot \tau(t)\|^2 = \bar{V}^2\|n(t)\|^2 - \|\bar{V}_p \cdot n(t)\|^2.$$

To determine the fluid velocity $\bar{V}$, we extrapolate $\varepsilon = \mathrm{sign}[\bar{V}_3 \cdot n(t)]$, where $\bar{V}_3$ is the fluid velocity at internal node s_3 (see Figure 1).

Finally one gets

$$\bar{V} = \frac{[\bar{V}_p \cdot n(t)]n(t) + \varepsilon\|\bar{V}\cdot \tau(t)\|\tau(t)}{\|n(t)\|}.$$

The field w_i at node S_i is then defined as the mean of the boundary field $\bar{w}$ on the left and right sides of node S_i, weighted by non-uniform mesh spacings.[28,29]

8. NUMERICAL RESULTS

To assess the Euler solver, calculations were performed for two AGARD aerofoils,[30] the NACA64A006 and NACA64A010 aerofoils, in the frequently critical transonic speed regime. As a first step the implicit method is used to compute as a limit the steady flows over the aerofoils.

In this case a local time step is used to enhance the convergence rate and internal dissipation in order to avoid spurious oscillations. The local time step is such that the local CFL number is uniform all over the spatial mesh and does not vary in time throughout the pseudo-unsteady evolution. As described in Reference 31, we compute for each element a time step Δt_T using the element dimensions. Here the element dimensions correspond to the square root of meas(T). This time step is used to perform the first stage (predictor) and the implicit stage. A nodal time step ΔT_S is then chosen to be the minimum of the ΔT_T corresponding to the elements surrounding this node.

For unsteady applications the nodal time step Δt_S is uniform over all the spatial mesh to preserve accuracy. As a consequence, a local Courant number follows and the maximum CFL number allowed is governed by the portions of the mesh with the smallest spacing.

8.1. NACA64A006 aerofoil with an oscillating flap

We have considered the transonic flow over the NACA64A006 aerofoil with a quarter-chord oscillating trailing edge flap. The freestream Mach number is $M_\infty = 0.875$ and the deflection angle of the flap is given by

$$\delta(t) = \delta_m + \delta_0 \sin(\omega t)$$

where the steady deflection angle of attack is $\delta_m = 0°$, the amplitude is $\delta_0 = 1°$ and ω is the angular frequency. The reduced frequency k defined by $\omega C/V_\infty$ (where C denotes the chord and V_∞ the freestream velocity) is equal to 0.470.

The computational mesh includes 4989 nodes, 224 of which lie on the aerofoil surface, and 8296 elements (Figure 2). the mesh extends to six chord lengths from the aerofoil. Away from

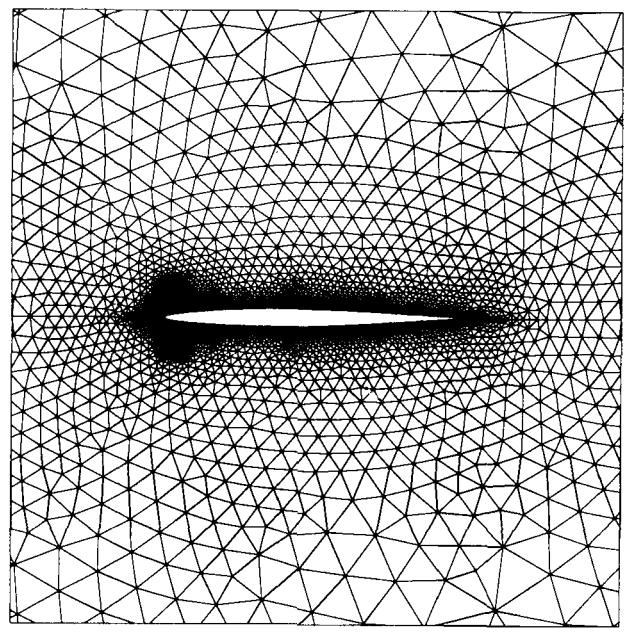

Figure 2. Computational mesh for the NACA64A006 aerofoil including 4989 nodes and 8296 elements (partial view)

the aerofoil the mesh size grows quickly in such a way that a mesh-enriching technique or a dynamic mesh must be used to capture shocks and slip lines properly.

The initial state is the steady flow over the aerofoil at rest in its initial location. It is computed by the present method from uniform initial data. The steady state calculation is achieved using 1947 interations (root-mean-square residues on the physical quantities less than 10^{-6}) and a CFL number of 4 in a CPU time of 250 s on a Cray XMP18 computer. This calculation is performed without taking into account the symmetry of the flow. The convergence history, the pressure distribution on the aerofoil and the entropy error are presented in Figure 3. Away from the leading edge the entropy error is very low.

Putting the flap in motion gives rise to an unsteady flow. The unsteady pressure distributions on the aerofoil are shown on Figure 4 at various moments of the periodic evolution. Only half of the cycle is presented, since a phase shift of 180° simply exchanges the pressure curves on the upper and lower surfaces in the present case. In the vicinity of the aerofoil the periodic regime is established after four cycles of oscillatory flap motion, as can be seen from the lift coefficient (Figure 5). Figure 6 shows the harmonic analysis of the unsteady upper pressure coefficient. The numerical results compare fairly well with experimental data given by Zwaan in Reference 32. Note that viscous effects are not taken into account in the numerical model. With a CFL number equal to 6, 2580 time steps are necessary to describe a cycle of oscillatory flap motion.

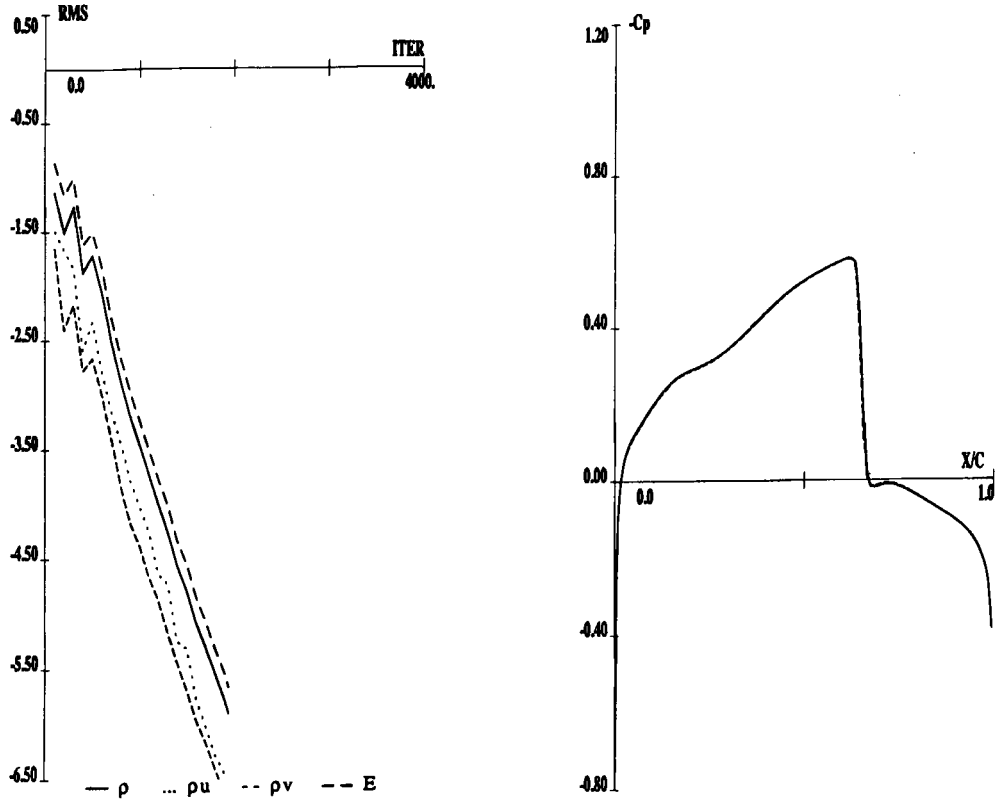

Figure 3. Steady solution around the NACA64A006 aerofoil at $M_\infty = 0.875$ and $\delta = 0°$: (a) convergence history; (b) steady pressure distribution; (c) entropy

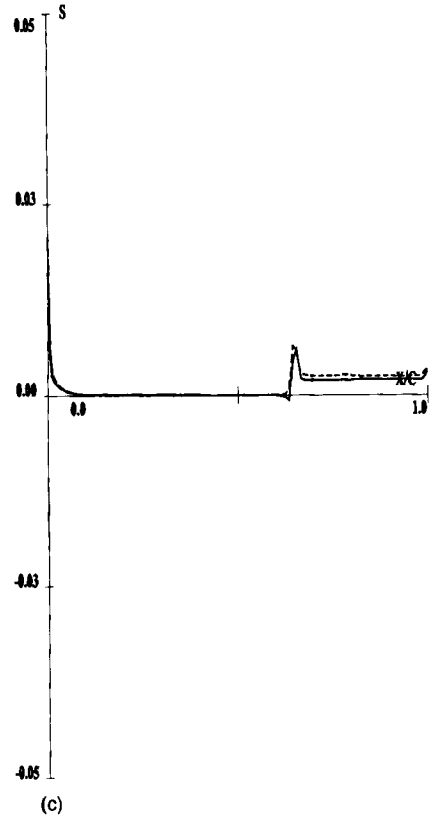

Figure 3. (*Continued*)

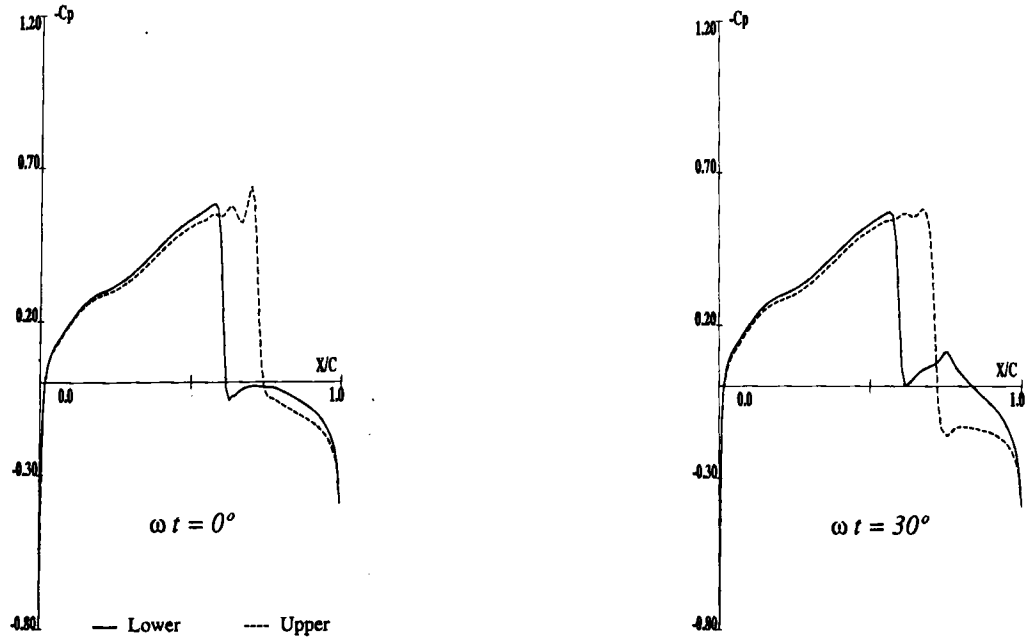

Figure 4. Unsteady pressure distribution for the NACA64A006 aerofoil with an oscillating flap at $M_\infty = 0.875$, $\delta(t) = \sin(\omega t)$ and $k = 0.470$

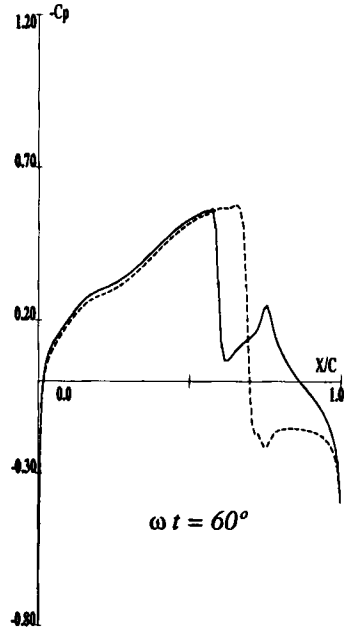

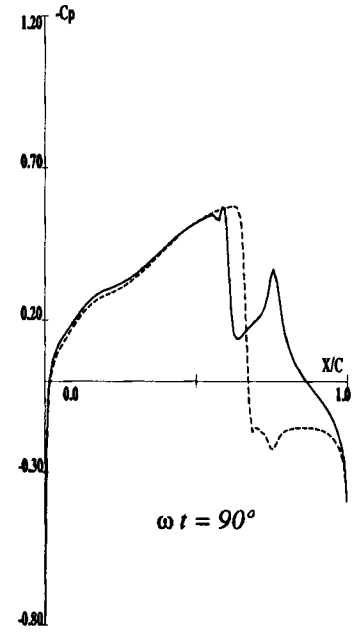

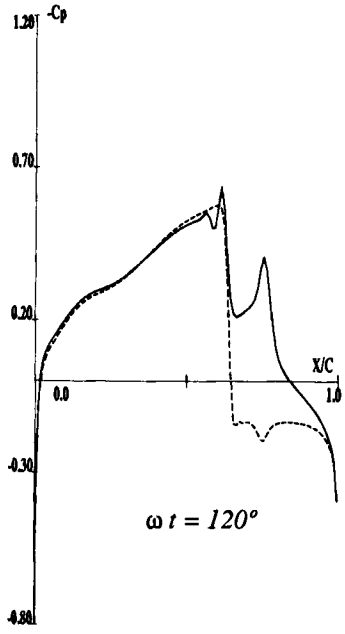

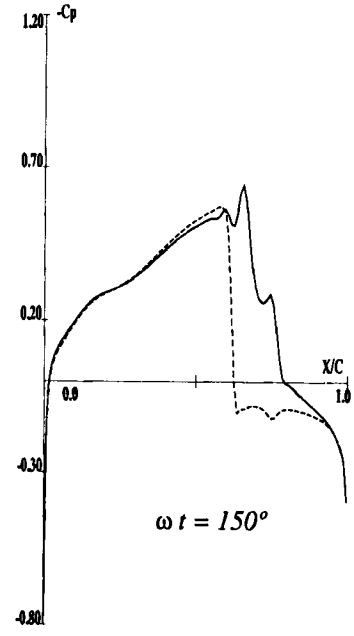

Figure 4. (*Continued*)

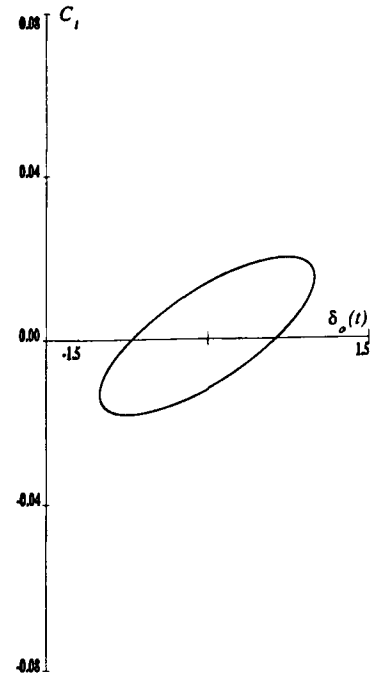

Figure 5. Lift coefficient after three cycles at $M_\infty = 0.875$, $\delta(t) = \sin(\omega t)$ and $k = 0.470$

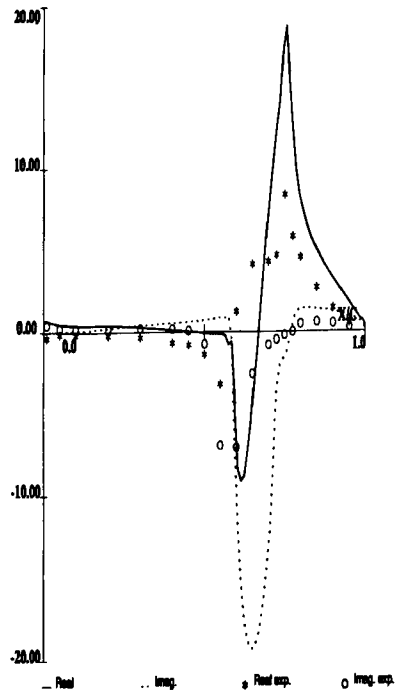

Figure 6. Harmonic analysis of the unsteady upper pressure coefficient: real and imaginary parts

The CPU time for the unsteady calculation is 220 s per cycle on the Cray XPM18 computer, so that it takes 880 s in total to achieve the whole calculation.

8.2. NACA64A010 aerofoil oscillating in pitch

The second application concerns the unsteady flow over the NACA64A010 aerofoil oscillating in pitch about the quarter-chord. The freestream Mach number M_∞ is equal to 0.796 and the aerofoil pitches about a mean angle of attack

$$\alpha(t) = \alpha_m + \alpha_0 \sin(\omega t)$$

where the steady angle of attack is $\alpha_m = 0°$, the amplitude is $\alpha_0 = 1°01'$ and the reduced frequency k is equal to 0.404.

The computational mesh includes 3813 nodes, 224 of which lie on the aerofoil surface, and 7343 elements (Figure 7). The initial steady state corresponding to the initial conditions $M_\infty = 0.796$ and $\alpha = \alpha_0 = 0°$ is presented on Figure 8. One can observe a small difference on the upper and lower pressure distributions which comes from the aerofoil definition.[30] The steady state calculation is achieved using 1886 iterations and a CFL number of 4 in a CPU time of 195 s. To specify the maximal shock wave evolution during the pitching motion, we present in Figure 9 the steady solution obtained for $\alpha_0 = 1°01$.

The steady field obtained for $M_\infty = 0.796$ and $\alpha = \alpha_0 = 0°$ is then used to initialize the unsteady calculation. The unsteady pressure distributions on the aerofoil are shown in Figure 10 at various moments of the periodic evolution (after three cycles). Figure 11 shows the variation in the lift coefficient with pitching angle for the whole time history of four calculated cycles of oscillations. The harmonic analysis of the unsteady upper pressure coefficient is shown in

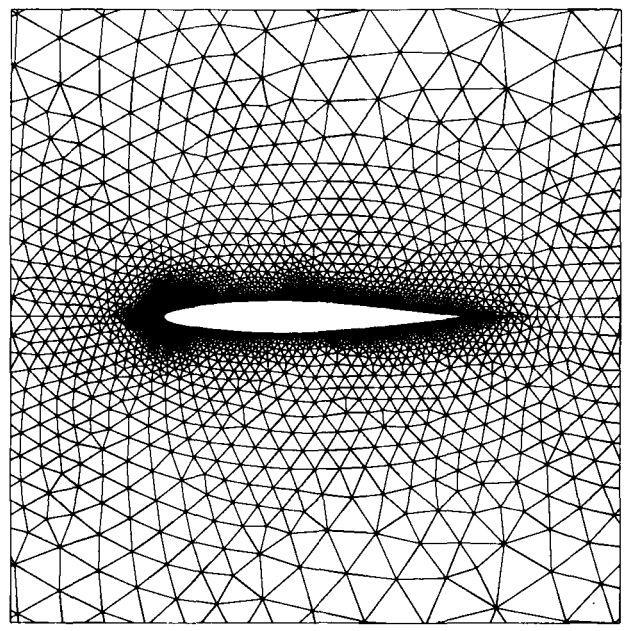

Figure 7. Computational mesh for the NACA64A010 aerofoil including 3813 nodes and 7343 elements (partial view)

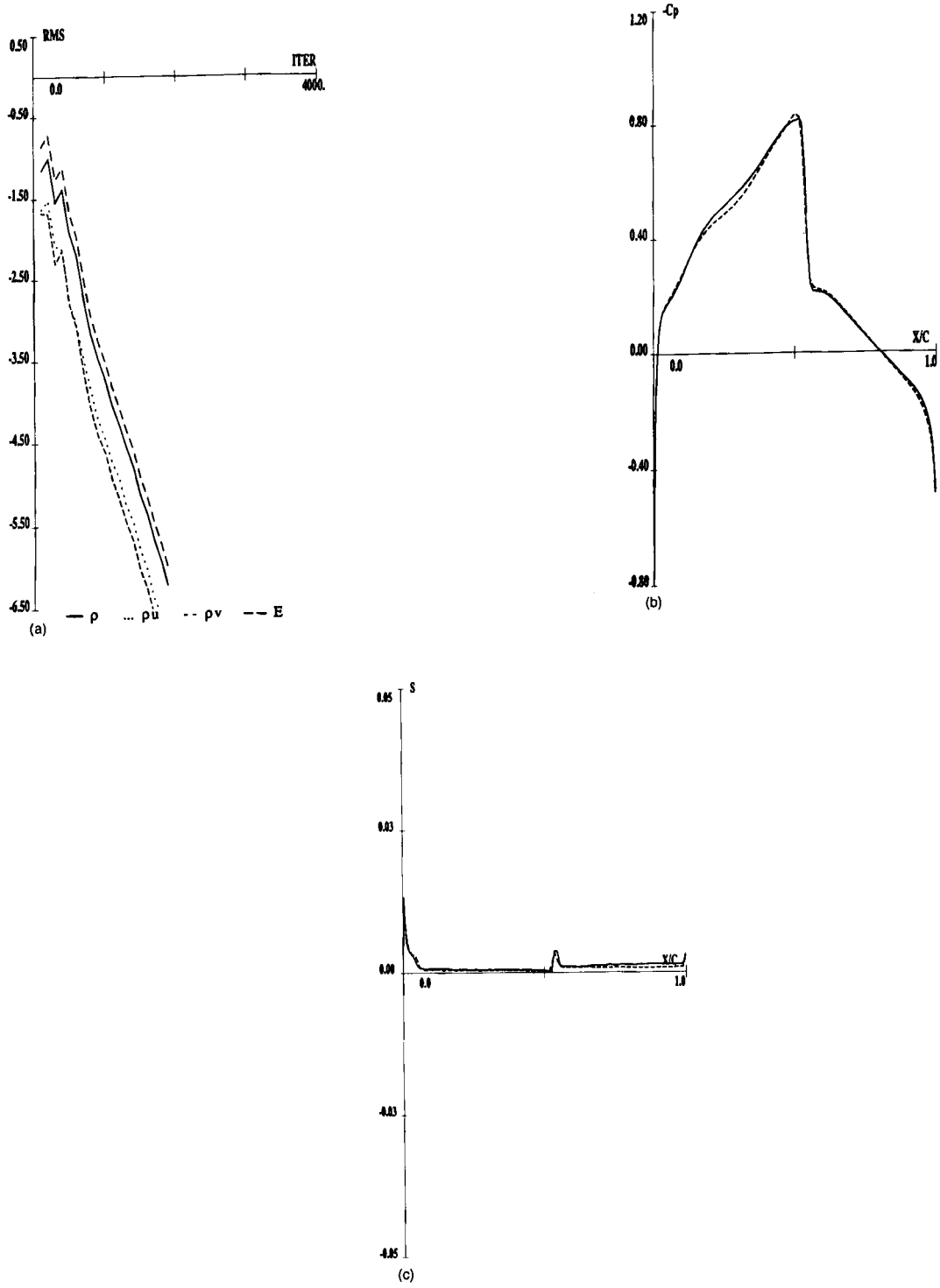

Figure 8. Steady solution around the NACA64A010 aerofoil at $M_\infty = 0.796$ and $\alpha = 0°$: (a) convergence history; (b) steady pressure distribution; (c) entropy

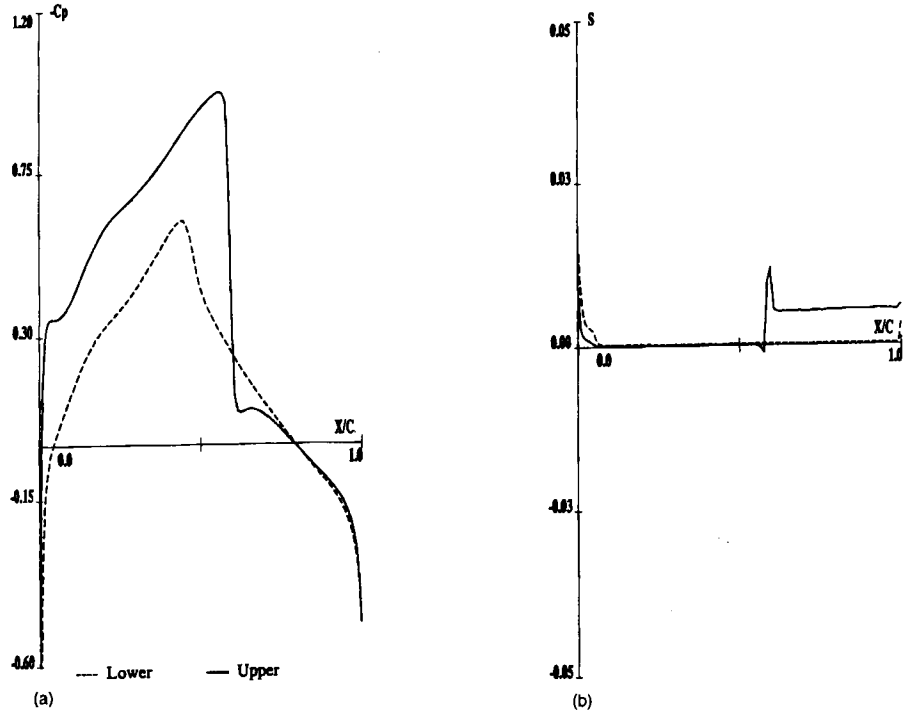

Figure 9. Steady solution around the NACA64A010 aerofoil ar $M_\infty = 0.796$ and $\alpha = 1°01'$: (a) pressure distribution; (b) entropy

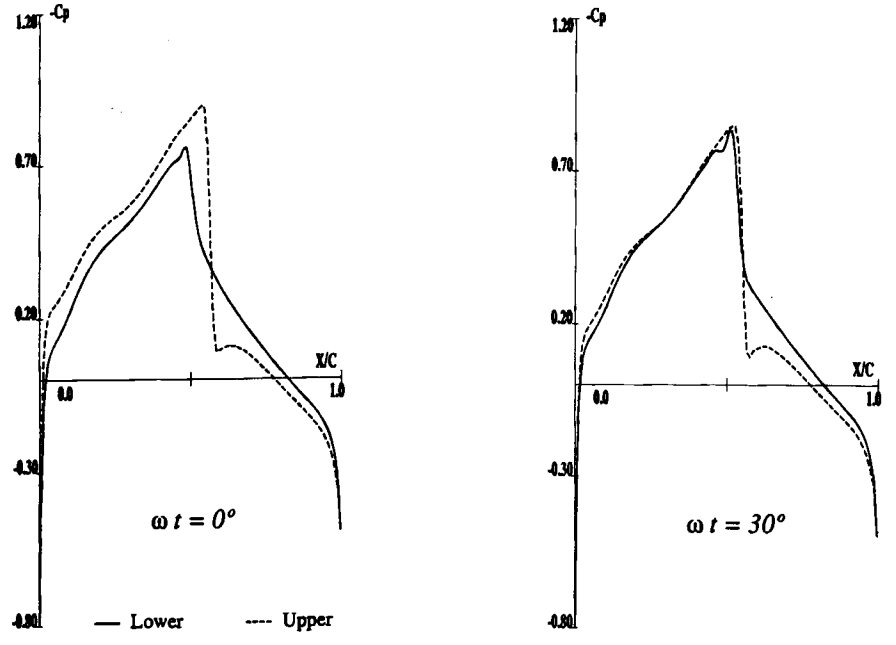

Figure 10. Unsteady pressure distribution for the NACA64A010 aerofoil oscillating in pitch at $M_\infty = 0.796$, $\alpha(t) = 1°01' \sin(\omega t)$ and $k = 0.404$

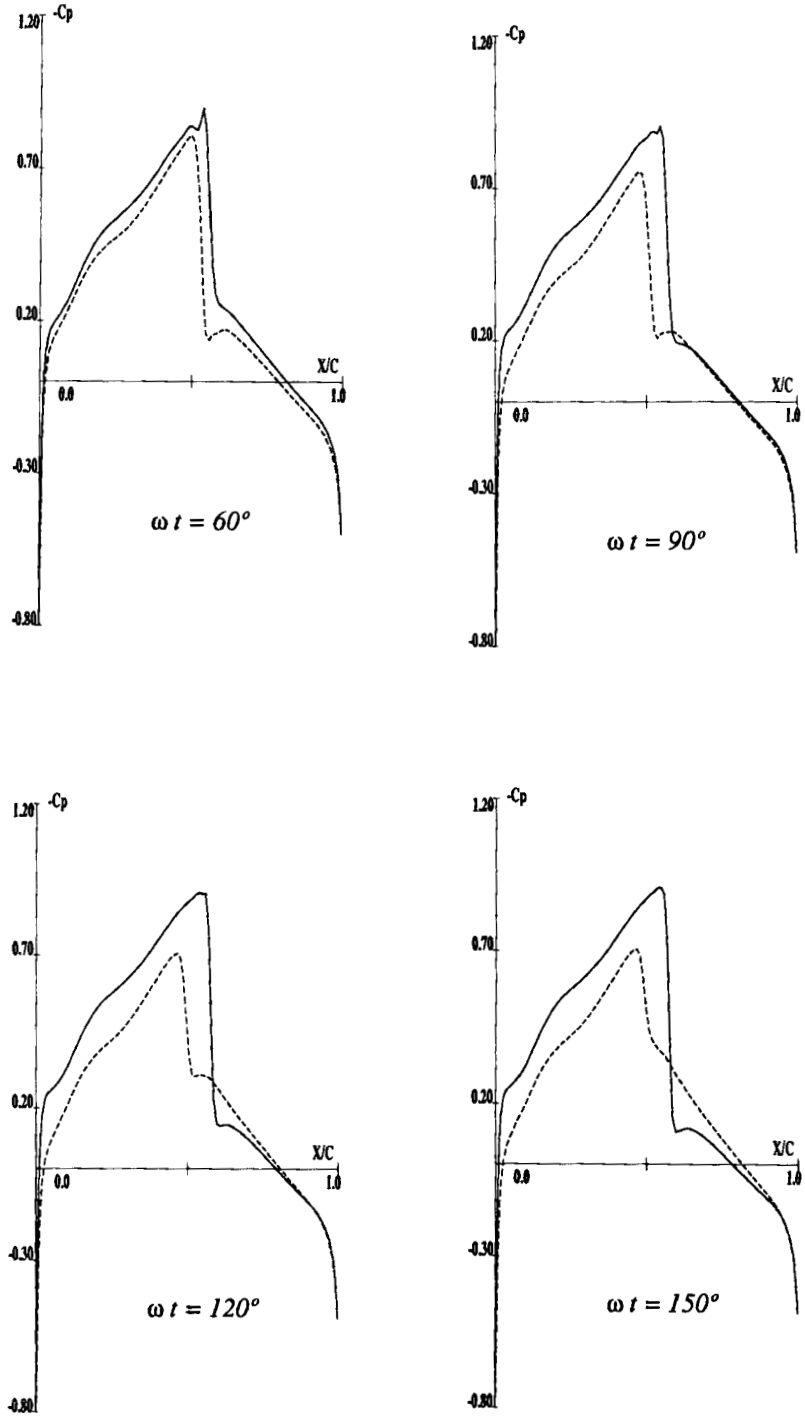

Figure 10. (*Continued*)

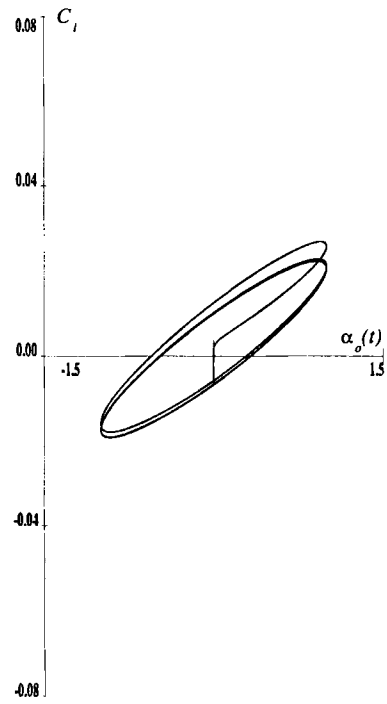

Figure 11. Time history of the lift coefficient for the NACA64A010 aerofoil oscillating in pitch at $M_\infty = 0.796$, $\alpha(t) = 1°01'\sin(\omega t)$ and $k = 0.404$

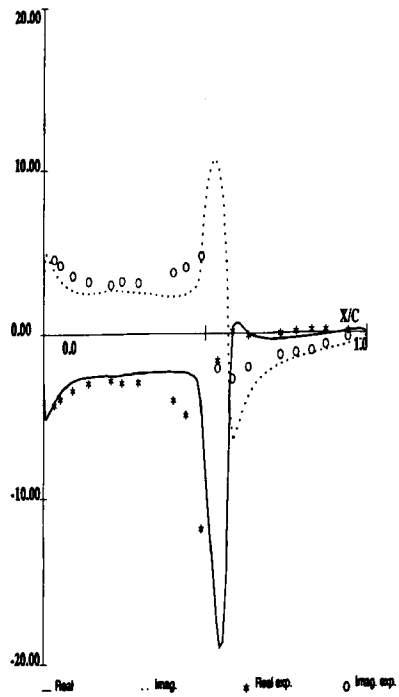

Figure 12. Harmonic analysis of the unsteady upper pressure coefficient: real and imaginary parts

Figure 12. For this case we have experimental data of Davis.[32] The numerical and experimental results show good agreement. The unsteady calculation is performed using a CFL number of 6. The number of time steps needed to calculate a cycle is 2790 and the global CPU time is 860 s.

9. CONCLUSIONS

An implicit finite element method has been developed for the solution of the 2D unsteady Euler equations. The flow solver involves an implicit time-dependent scheme with a finite element discretization for use on an unstructured mesh made up of triangles. Another significant aspect of the research is the implementation of boundary conditions on a solid mobile wall which allow us to keep a fixed mesh. With this solver no artificial viscosity is added to ensure the success of steady and unsteady calculations. As far as the unsteady case shown here is concerned, the results on the aerofoil surface fit fairly well with those reported in Reference 32.

As an application, the authors have recently used this implicit finite element method to calculate the internal flow of an inviscid fluid in two-dimensional turbine or compressor cascade blades. The first results seem to be promising.

The current effort is being directed towards extending this method to three-dimensional flows using tetrahedral grids for unsteady aerodynamic and aeroelastic analysis of complete aircraft configurations.

REFERENCES

1. M. Couston and J. J. Angelini, 'Solution of nonsteady two dimensional disturbance potential flow equation,' *ASME J. Fluid Eng.*, **101**, (1979).
2. J. W. Edwards and J. L. Thomas. 'Computational methods for unsteady transonic flows,' *AIAA Paper 87-0107*, 1987.
3. J. T. Batina, 'Unsteady transonic algorithm improvements for realistic aircraft applications,' *J. Aircraft*, **26**, 131–139 (1989).
4. F. Angrand, A. Dervieux, L. Loth and G. Vijayasundaram, 'Simulation of Euler transonic flows by means of explicit finite element-type schemes,' *INRIA Res. Rep. 250*, 1983.
5. O. C. Zienkiewicz, R. Lohner and K. Morgan, 'High speed inviscid compressible flow by the finite element method,' *V-MAFELAP Conf.*, May 1984.
6. V. Selmin, 'Finite element solution of hyperbolic equations,' *INRIA Res. Rep. 655, 706 and 708*, 1987.
7. W. Koschel, M. Lotzerich and A. Vornbeger, 'Solution on unstructured grids for the Euler and Navier–Stokes equations,' *AGARD CP 437*, 1988.
8. L. Fezoui and B. Stoufflet, 'A class of implicit upwind schemes for Euler simulations with unstructured meshes,' *J. Comput. Phys.*, **84**, 174–206 (1989).
9. D. J. Mavriplis, 'Multigrid solution of the 2-D Euler equations on unstructured triangular meshes,' *AIAA J.*, **26**, 824–831 (1988).
10. A. Jameson, T. J. Baker and N. P. Weatherill, 'Calculation of inviscid transonic flow over a complete aircraft,' *AIAA Paper 86-0103*, 1986.
11. V. Billey, A. Dervieux, L. Fezoui, J. Periaux, V. Selmin and B. Stoufflet, 'Recent improvements in Galerkin and upwind Euler solvers and applications to 3-D transonic flow in aircraft design,' *Comput. Methods Appl. Mech. Eng.*, **75**, 409–414 (1989).
12. G. D. Mortchelewicz, 'Résolution de équations d'Euler instationnaires en maillages non structurés,' *La Recherche Aérospatiale 1989-6*, 1989, pp. 30–100.
13. O. Hassan, K. Morgan and J. Peraire, 'An adaptive implicit/explicit finite element scheme for compressible viscous high speed flows,' *AIAA Paper 89-0363*, 1989.
14. J. T. Batina, 'Unsteady Euler algorithm with unstructured dynamic meshes for complex aircraft aeroelastic analysis,' *AIAA Paper 89-1189*, 1989.
15. R. Lohner, K. Morgan, J. Peraire and M. Vahdati, 'Finite element flux-corrected transport (FEM-FCT) for the Euler and Navier–Stokes equations,' *Int. j. numer. methods fluids*, **7**, 1093–1109 (1987).
16. A. Lerat, 'Une classe de schémas aux différences implicites pour les systèmes hyperboliques de lois de conservation,' *C. R. Acad. Sci. Paris A*, **288**, 1033–1036 (1979).
17. Lerat, 'Sur le calcul des solutions faibles des systèmes hyperboliques de lois de conservation à l'aide de schémas aux différences,' *Publ. ONERA 1981-1*, 1981.
18. A. Lerat, J. Sidès and V. Daru, 'An implicit finite volume method for solving the Euler equations,' *Lecture Notes in Physics*, Vol. 170, Springer, Berlin, 1982, pp. 343–349.
19. A. Lerat and J. Sidès, 'Efficient solution of the steady Euler equations with a centered implicit method,' in K. W. Morton and M. J. Baines (eds), *Numerical Methods in Fluid Dynamics III*, Clarendon, Oxford, 1988, pp. 65–86.

20. A. S. Sens, 'Calcul d'écoulements transsoniques instationnaires par résolution implicite centrée des équations d'Euler sans viscosité artificielle,' *Note Tech. ONERA 1990-8*, 1990.
21. A. Lerat and R. Peyret, 'Proriétés dispersives et dissipatives d'une classe de schémas aux différences pour les systèmes hyperboliques non linéaires,' *La Recherche Aérospatiale 1975-2*, 1975, pp. 61–79.
22. A. Lerat, "Difference methods for hyperbolic problems with emphasis on space-centered approximations,' *Lecture Series 1990-03, Von Karman Institute for Fluid Dynamics*, Brussels, 1990.
23. P. Joly, 'Méthode de gradient conjugué,' in *Cours d'Analyse Numérique*, Paris VI.
24. H. Viviand and J. P. Veuillot, 'Méthodes pseudo-instationnaires pour le calcul d'écoulements transsoniques,' *Publ. ONERA 1978-4*, 1978.
25. A. Lerat and J. Sidès, 'Implicit transonic calculations without artificial viscosity or upwinding,' *Notes Numer. Flud Mech.*, **26**, 227–250 (1989).
26. J. Sidès, 'Calcul d'écoulements transsoniques instationnaires à l'aide d'une méthode numérique implicite de résolution des équations d'Euler, *La Recherche Aérospatiale 1985-2*, 1985, pp. 89–111.
27. G. D. Mortchelewicz, 'Résolution des équations d'Euler tridimensionnnelles instationnaires en maillages non structurés,; *La Recherche Aérospatiale 1991-6*, 1991, pp. 17–25.
28. P. L. Roe, 'Error estimates for cell-vertex solutions of the compressible Euler equations,' *ICASE Rep. 87-6*, 1987.
29. E. Turkel, 'Accuracy of schemes with non uniform meshes for compressible fluid flows,' *ICASE Rep. 85-43*, 1985.
30. AGARD, 'AGARD two dimensional aeroelastic configurations,' *AGARD Advisory Rep. 156*, 1979.
31. K. Morgan and J. Peraire, 'Finite element methods for compressible flows,' in *Lecture Series 1987-04*, Von Karman Institute for Fluid Dynamics, Brussels, 1987.
32. AGARD, 'Compendium of unsteady aerodynamic measurements,' *AGARD Rep. 702 and Addendum 1*, 1982.